International Journal of Thermophysics, Vol. 4, No. 3, 1983

High Speed Scanning Calorimetry for Amorphous Alloys

B. Hopstadius[1] and G. Bäckström[1]

Received July 8, 1983

A high speed scanning calorimeter has been developed for simultaneous measurements of heat capacity and electrical resistivity of thin strips. The system was designed for amorphous alloys but can be used for other materials as well. The specimen is heated by an electrical current at rates ranging from 250 to 40,000 $K \cdot s^{-1}$, and the temperature is sensed by an IR pyrometer ranging down to room temperature. The maximum data acquisition rate is 50 kHz. Operational characteristics of the system are given, and various phenomena that affect design and operation are discussed. Data are taken for some Metglas alloys. Glass transition and crystallization temperatures as well as rough viscosity data are evaluated. At high heating rates the glass transition is spread over a wide temperature range. The formation of metastable crystalline phases can be bypassed so that stable phases form directly from the amorphous state.

KEY WORDS: amorphous state; calorimetry; crystallization; glass transition (glasses); specific heat of solids; temperature measurements.

1. INTRODUCTION

Although glass has been known for centuries, it is only during the past decade that metallic materials of glassy structure have become available. They are produced by quenching alloys from the melt at rates of the order of 10^6 $K \cdot s^{-1}$ [1]. When a liquid is cooled, its viscosity increases rapidly, and at a sufficiently high cooling rate, viscosity completely inhibits crystallization. Below the so-called glass transition temperature, T_g, the material is no longer in thermodynamic equilibrium and possesses excess free energy.

The specific heat of metallic glasses has been studied by differential thermal analysis (DTA) and by differential scanning calorimetry (DSC) at heating rates up to 50 $K \cdot s^{-1}$. The results show that the specific heat

[1]Department of Physics, University of Umeå, S-901 87 Umeå, Sweden.

0195-928X/83/0900-0235$03.00/0

capacity, c_p, increases rapidly in the region of the glass transition, passes through a maximum, and then drops slowly [2]. We may define T_g as the temperature where c_p reaches, say, half of its maximum increment. Studies of the c_p anomaly at different scanning speeds show, however, that T_g depends appreciably on the rate of heating.

According to a plausible kinetic theory of glass transitions [3], no peak in c_p should arise if the calorimeter heating rate is less than the cooling rate at which the glass was produced. This general conclusion has been verified in cases of organic liquids [4]. A crucial question is whether a modified theory is required for metallic glasses, in view of the peak actually observed. An experimental complication occurs in the case of amorphous alloys in that they crystallize at a temperature, T_x, which is only slightly above T_g. This feature may have obscured findings concerning the behavior of c_p at the glass transition. It would be of interest to measure amorphous alloys at high scanning speeds for at least three reasons. First, such experiments might shed new light on the anomaly in c_p. Second, it would yield information on the rate dependence of T_g and T_x. Third, the crystallization process and the phases appearing have never been studied at heating rates approaching those used during quenching of these alloys.

Metallic glasses can be rapidly heated by a high electric current. This procedure has often been used in measurements of heat capacity and other thermophysical properties of metals at rates up to 10^9 K $\cdot$ s^{-1} and temperatures up to 9000 K [5, 6]. The temperature is usually measured optically by a pyrometer viewing a black body cavity in the specimen, providing convenient temperature calibration. In some applications, where a cavity cannot be formed, radiation from the surface has been used and constant emissivity assumed but not checked experimentally [7, 8].

High speed heat capacity measurements have so far only been made at high temperatures. The lowest operation temperature known to us is 800 K [9]. The pulse heating technique has also been applied to an amorphous alloy in a measurement of viscosity above T_g [10]. The heating rate was 130 K $\cdot$ s^{-1}, and the temperature was measured via the specimen resistivity, in the range where that resistivity could be determined quasi-statically. At higher temperatures no temperature measurement was done. The aim of the present work was to develop a calorimeter for scanning rates much higher than those attainable with a DSC, the temperature being sensed by a pyrometer.

2. MEASUREMENT SYSTEM

The design of the apparatus is presented schematically in Fig. 1. It is basically similar to systems used elsewhere [6], but some details depend on

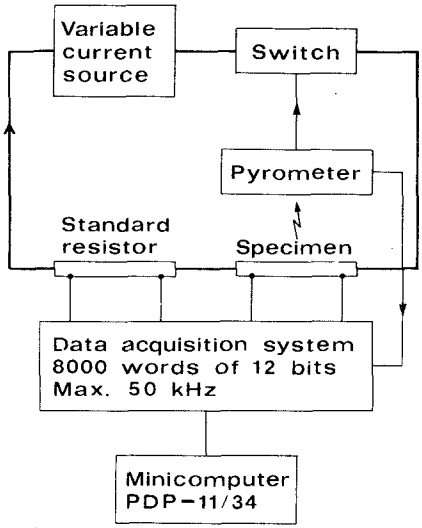

Fig. 1. Block diagram of high speed calorimeter.

our application to thin strips. The current source consists of two Kepco B32-30Rs, yielding a maximum of 80 A. Current is supplied to the specimen via massive copper clamps, and a similar pair of clamps is used for extracting the voltage drop (Fig. 2). The upper clamps are movable in order to allow for thermal expansion and may be spring loaded to keep the specimen under tensile stress. Specimens are typically 65 mm long, 2–4 mm wide, and 0.025–0.10 mm thick, the potential taps being 35 mm apart. A thermocouple, attached to a clamp, measures the initial temperature of the specimen.

The specimen and its holder are mounted in a metal chamber which can be evacuated to 10^{-3} Pa. Infrared radiation from the middle part of the specimen reaches the pyrometer through a sapphire window. Focusing is achieved by a system of two identical Ge lenses, and the aperture is controlled by circular baffles, introduced between the lenses. The pyrometer is a photovoltaic InSb detector, cooled by liquid nitrogen. Its area is 0.1 mm^2, and the effective wavelength range is 1–5.5 μm. Its short time constant, 1 μs, is an important feature in this application. The specimen is fixed in the chamber, but the pyrometer can be moved to focus on the middle of the specimen. The semiconductor switch in series with the current supply closes on manual command and opens when the pyrometer voltage reaches a preset level, thus limiting the specimen temperature.

The data acquisition system has an analogue multiplexer and a 12-bit A/D converter. Input channels are scanned sequentially, each scan starting

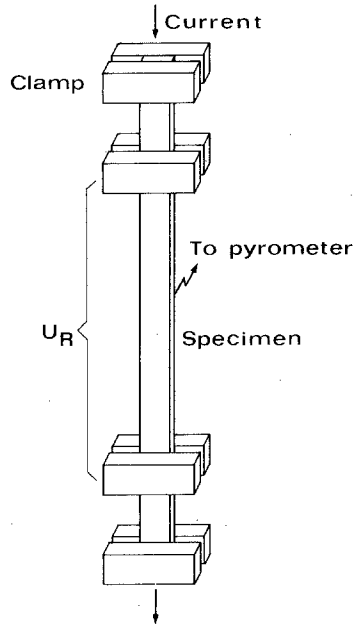

Fig. 2. Specimen holder for high speed calorimeter. The dimensions are not to scale.

on command from a preset clock. The system has a buffer memory, and its contents are transferred after the experiment to a PDP-11/34 computer, where all data reduction is carried out. Static measurements and calibrations of the data acquistion system are made using a Hewlett-Packard 3456A voltmeter.

3. DATA PROCESSING

The data acquisition system scans consecutive channels at a time increment of 20 μs. We usually set the system to measure cycles of three channels, corresponding to the voltages from the manganin resistor (U_N), from the specimen (U_R), and from the pyrometer (U_T). The time interval between cycles (Δt) may be selected. We first reduce the measurements of U_N and U_R to the same time as U_T by linear interpolation. The temperatures, T, are then calculated from U_T using one of the transfer functions discussed below.

Relative values of the resistivity are approximately given by $R = U_R/U_N$, but a correlation must be applied, since U_R is proportional to the total resistance between clamps. The resistivity should refer to the middle of the strip, where the temperature is measured, since the ends are

at room temperature. We preferred heavy copper clamps to ordinary, spot welded wire taps, since the former yield better defined thermal boundary conditions. In cases where this correction is important we have calculated the local resistivity by solving numerically the equation of heat conduction [11].

An approximation to the relative specific heat capacity is obtained from $U_R U_N \Delta t/\Delta T$, the time interval being taken symmetrically. As in the case of resistivity, we correct U_R, where necessary, for cooling from the ends. Absolute values of both resistivity and c_p may of course be obtained by trivial additional measurements, but it is more convenient to normalize data using known results. Radiation heat losses can be calculated using measured cooling rates. These can be used for c_p correction on heating and for c_p calculation on cooling [12].

4. PYROMETER CALIBRATION

4.1. Theory

There are two main difficulties associated with pyrometer measurements on amorphous alloys. First, the temperatures of interest range from 300 K, where the radiation intensity is small. Second, the specimens are available as strips and cannot easily be shaped into tubes. This makes it impracticable to implement a black body cavity within the specimen, as has been done in previous work [5, 6].

According to a standard pyrometer theory the output voltage, U_T, may be written as

$$U_T = C_1 \int \frac{\epsilon(\Lambda) S(\Lambda)\, d\Lambda}{\Lambda^5 \left[\exp(c_0/\Lambda T) - 1\right]} \tag{1}$$

where C_1 and c_0 are constants, ϵ is the emissivity, Λ is the wavelength, and $S(\Lambda)$ is the combined spectral response function of the lens system and the radiation detector. The pyrometer wavelength window (1–5.5 μm) only partly accepts the radiation spectrum emitted in the range 300–1300 K. At low temperatures the accepted wavelengths are far from the spectral peak, and we can replace the pyrometer window by a typical wavelength. With this approximation and neglecting the unity term within brackets, Eq. (1) reduces to

$$U_T = \epsilon C \exp(-K/T) \tag{2}$$

where C and K are constants. For computational purposes the real relationship may conveniently be written in the same form, with K replaced by

$f(T)$, where $f(T)$ is a slowly varying function, practically constant for small T. The function $f(T)$ may be obtained by integration of Eq. (1) using measured values of $S(\Lambda)$. We preferred, however, to measure $f(T)$ directly at various apertures using a black body oven radiating at temperatures determined by a thermocouple.

4.2. Calibration Assuming Constant Emissivity

With $f(T)$ known from black body measurements, it suffices to determine the constant emissivity, ϵ. The simplest procedure is to determine ϵ using a known transition temperature, i.e., the Curie point. In a separate paper [13] we have shown that for Fe, the Curie point is independent of heating rate, and we assume this to hold for amorphous alloys as well. Curie points for these materials have been determined quasi-statically and may be detected in our curves of resistance versus temperature or, alternatively, of temperature versus time. The kinks are somewhat smeared, however, yielding a random error of 5 K or more in the calibration temperature (see Figs. 3a–6a and 8b below).

As an alternative calibration procedure, we measured the resistance quasi-statically at a few temperatures up to 470 K. These data were then compared to resistance values obtained in subsequent dynamic experiments, which permitted us to determine the emissivity using the known $f(T)$. This calibration procedure was found to be more accurate but also more tedius.

4.3. Calibration Allowing for $\epsilon(T)$ Variation

According to theories for thermal emissivity [14], ϵ is related to the surface structure and the electrical resistivity, R, and hence is to some extent temperature dependent. We have thus attempted to calibrate temperatures without assuming constant emissivity. The strategy was to use a standard surface layer of Pt on all specimens, thin enough to have a negligible influence on R and c_p, but thick enough to be opaque in the infrared. We also planned to deposit this standard Pt layer on a Pt strip that could be used as a resistance thermometer in a dynamic experiment. Resistance values had, however, to be corrected for the variation of temperature along the strip, assuming the temperature at the inner edges of the clamps to be constant. Calculations of the temperature distributions at various times were made by the numerical methods mentioned above. These calculations required literature values of the thermal conductivity, $\lambda(T)$, and the heat capacity per unit volume, ρc_p. The errors in λ and ρc_p contributed very little to the temperature error, since the entire end effect was at most a few percent of T. Electrical resistivity values were taken from standard tables for platinum thermometers.

The difficulty with the above calibration procedure proved to be the instability of evaporated Pt layers. In the first evaporation, platinum and iron specimens were covered with a 70 nm thick layer of Pt, unfortunately not thick enough to be opaque. The next trial resulted in a thickness of 220 nm, but although this layer was opaque and adhered well to iron specimens, it did not stick to a Pt strip.

We measured U_T versus T for a Pt specimen with a 70 nm layer and used the resulting function $f(T)$ for iron specimens with a 220 nm layer. Heating the iron specimen to 1100 K produced a marked change in emissivity, observed as a shift in the Curie temperature by 80 K from first to second scan. The emissivity drift, no doubt due to recrystallization, decreased in subsequent heating cycles, and the emissivity eventually reached a stable value. Under these conditions we investigated the effect of heating rate on the Curie temperature [13]. The instability of Pt layers made them unsuitable for amorphous alloys, and we are now trying to find other materials which are more stable in this application.

4.4. Resolution and Accuracy

The resolution in the electrical measurements is limited by that of the A/D converter (0.025% of full scale), since no bridge arrangement or zero suppression was used. As a result bit steps were sometimes noticeable (Fig. 3b), but the precision is still considered acceptable for our purposes. The finite voltage resolution, of course, also influences the pyrometer measurements, but in this case the scatter is mostly caused by noise from the InSb detector and its preamplifier. By differentiating Eq. (2), we see that the scatter in T decreases dramatically at higher temperatures for a given noise level. The best temperature resolution is obtained at the upper end of the temperature range limited by the aperture chosen. The largest aperture gives a scatter of 0.04 K (standard deviation) at 570 K, and a smaller aperture gives 0.15 K at 950 K.

In order to estimate the total random error, we scanned some samples of Metglas 2605SC with heating rates in the range 250–29,000 $K \cdot s^{-1}$. The Curie temperature, T_c, was evaluated from the kink in the $T(t)$ plot (Figs. 3a–5a). The test thus included random errors from the apparatus, specimen cleaning, focussing, emissivity variations between samples, and the evaluation of kinks. The standard deviation in T_c for eight samples was 3.5 K.

Unfortunately, we have not yet been able to establish an absolute temperature scale of comparable accuracy, the estimated limits being ± 15K. An additional source of error arises from insufficient knowledge of T_c, which depends on the thermal history of the sample [15]. Also, the emissivity must so far be taken as constant against temperature, although further development of evaporated layers may eventually make it possible to take a variation into account.

5. MEASUREMENTS AND DISCUSSION

We have so far obtained preliminary data for a series of Metglas alloys from Allied Chemical (New Jersey, U.S.A.), as listed in Table I. The temperature scale was calibrated as described in Section 4.2 for allows with a detectable Curie point. In some cases we have used the emissivity value from another alloy with about the same resistivity and surface structure. Figures 3a, 4a, and 5a show plots of T versus time for the alloy 2605SC at three different heating rates ranging from 250 to 29,000 $K \cdot s^{-1}$. Figures 3b, 4b, and 5b show R and c_p versus T for the same scans. The temperatures T_c, T_g, and T_x can be identified in the plots, and some data are compiled in Table II. We find that T_x increases more than T_g with increasing heating rate, in agreement with results at much lower rates [10, 16]. For 2605SC, T_c is most easily detected in the plot of T versus time. The small increase in slope with increasing heating rate in the $R(T)$ plots is due to end cooling.

The apparent c_p is dependent on the thermal history of the sample. If the heating rate is much smaller than the cooling rate employed on glass formation, relaxation can yield a minimum in the $c_p(T)$ plot before the increase usually associated with the glass transition [17]. Figures 3b–5b have no such evidence for early relaxation. Chen and Turnbull [18] made DSC measurements on $Au_{77}Ge_{13.6}Si_{9.4}$ with heating rates of 2.5–40 K ·

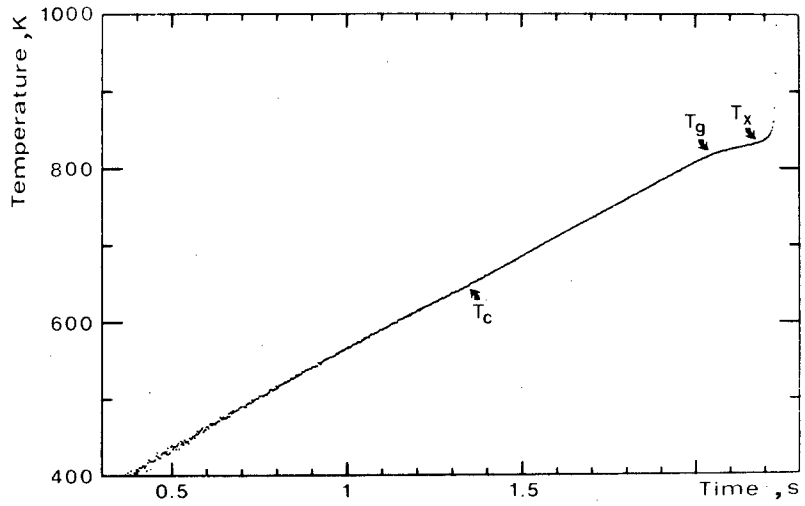

Fig. 3. Results obtained for Metglas 2605SC. The heating rate is 250 $K \cdot s^{-1}$. T_c = Curie point; T_g = glass transitions; T_x = onset of crystallization. (a, *above*) Temperature vs time. (b, *opposite*) Electrical resistance and heat capacity vs temperature. The specimen is under tensile stress. (For Figs. 3–9, parts a and b refer to the same temperature scan.)

Table I. Alloys Studied and Basis for Temperature Calibration

Metglas	Nominal composition (at.%)	Temperature calibration
2605	$Fe_{80}B_{20}$	$T_c = 647$ K
2605SC	$Fe_{81}B_{13.5}Si_{3.5}C_2$	$T_c = 643$ K
2605CO	$Fe_{67}Co_{18}B_{14}Si_1$	Same emissivity as 2605SC
2826	$Fe_{40}Ni_{40}P_{16}B_4$	$T_c = 510$ K
2826A	$Fe_{32}Ni_{36}Cr_{14}P_{12}B_6$	Same emissivity as 2826

min^{-1} and found that the slope of the $c_p(T)$ plot at the glass transition decreased with increasing heating rate. Our results show the same tendency at much higher heating rates.

The specimen in Fig. 3 is under tensile stress and elongates on heating as the viscosity decreases in the glass transition region before crystallization. This clearly demonstrates that the increase in c_p is connected with a drastic increase in viscosity. No previous, simultaneous measurements of these properties are known to us. Takamori et al. [19] made dynamic viscosity measurements on Metglas 2826. They found a sharp decrease after the glass transition and a sharp increase at the onset of crystallization. At a heating rate of 10 $K \cdot min^{-1}$ the viscosity changed by one order of magnitude in either direction over a temperature range of 15 K just below T_x. For some scans, we made rough measurements of tensile stress and excess resistance due to elongation. From this we calculated the viscosity

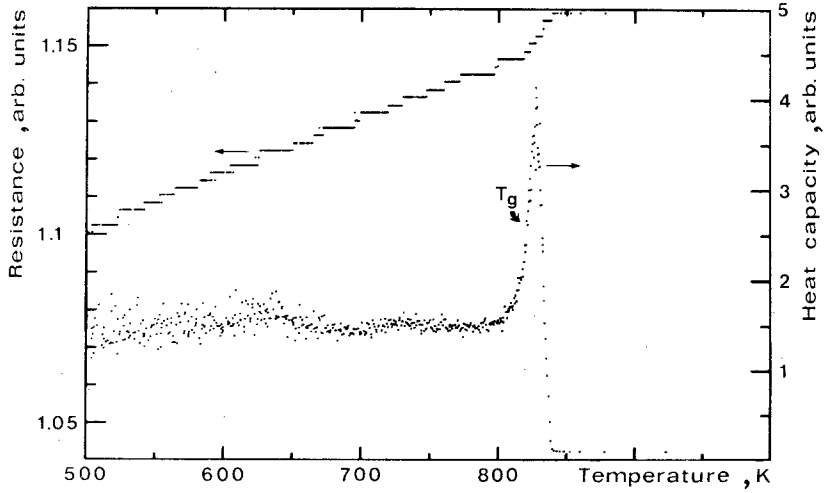

Fig. 3b.

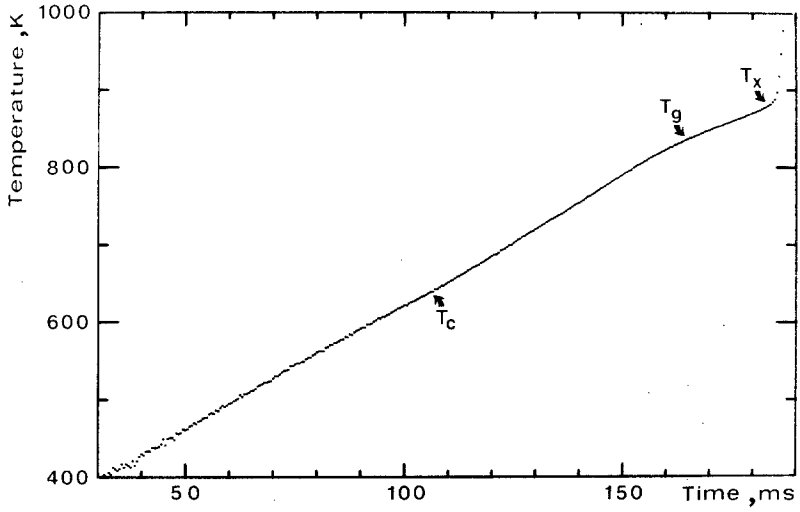

Fig. 4. Results obtained for Metglas 2605SC. The heating rate was 3500 $K \cdot s^{-1}$. (a, *above*) Temperature vs time. (b, *opposite*) Electrical resistance and heat capacity vs temperature.

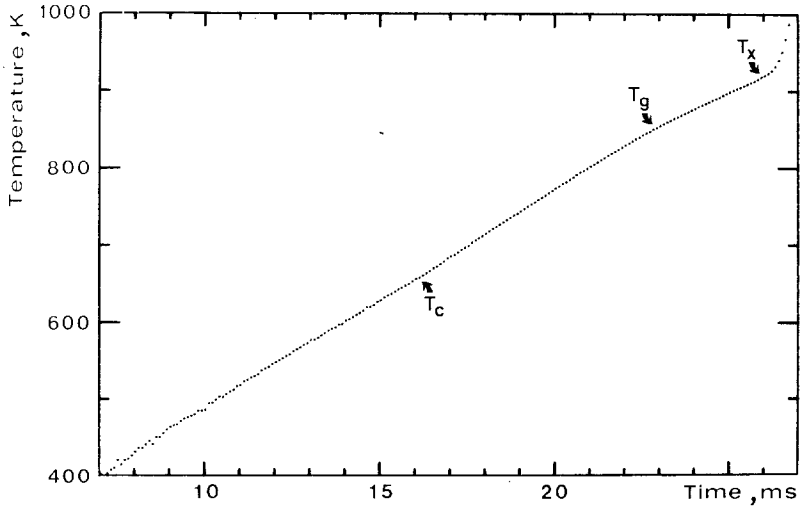

Fig. 5. Results obtained for Metglas 2605SC. The heating rate was 29,000 $K \cdot s^{-1}$. (a, *above*) Temperature vs time. (b, *opposite*) Electrical resistance and heat capacity vs temperature.

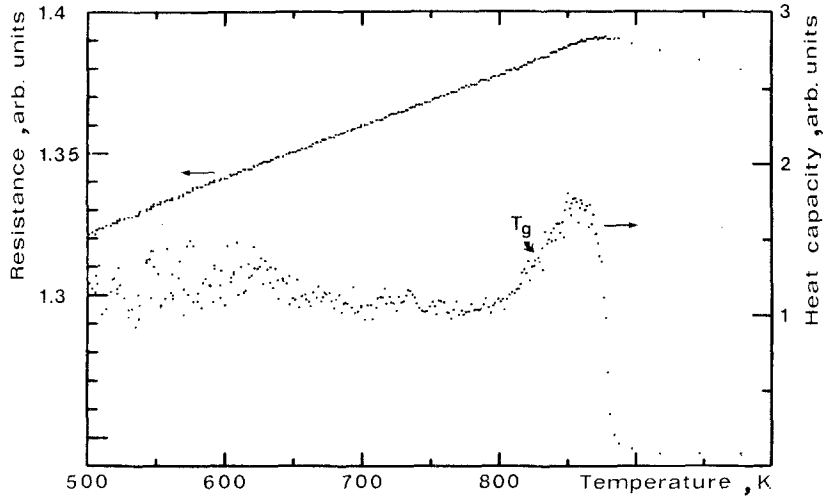
Resistance ,arb. units
1.4
1.35
1.3
Heat capacity ,arb. units
3
2
1
T_g
500
600
700
800
Temperature ,K

Fig. 4b.

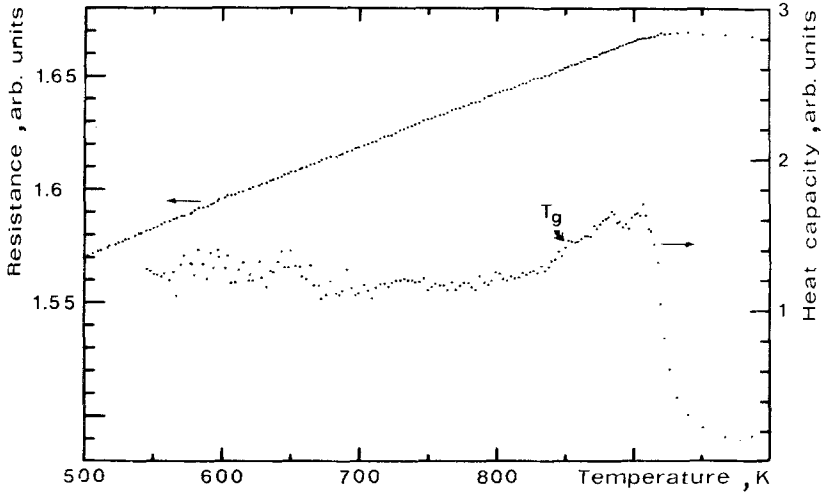
Resistance ,arb. units
1.65
1.6
1.55
Heat capacity ,arb. units
3
2
1
T_g
500
600
700
800
Temperature ,K

Fig. 5b.

Table II. Data from Scans on Metglas 2605SC Shown in Figures 3–5

Heating rate ($K \cdot s^{-1}$)	T_g (K)	T_x (K)	Maximum self-heating rate ($K \cdot s^{-1}$)
250	821	831	2×10^4
3500	830	874	7×10^4
29,000	855	923	3×10^5

just below T_x to be 2×10^6 N · s · m^{-2} at a heating rate of 250 K · s^{-1} (Fig. 3) and 5×10^4 N · s · m^{-2} at 29,000 K · s^{-1}. Anderson and Lord [10] in a similar experiment on Metglas 2826 obtained the viscosity 4×10^5 N · s · m^{-2} just above T_g at 130 K · s^{-1}. No viscosity measurements on amorphous alloys with higher heating rates, i.e., at temperatures higher above T_g, are known to us.

When crystallization starts, enthalpy will be released, increasing the specimen temperature. The maximum self-heating rate may be taken as a rough measure of the reaction rate, and it rapidly increases with crystallization temperature (Table II).

Figures 6–9 show recordings for the remaining alloys listed in Table I. In Figs. 6a and 8b Curie points can be detected. In Fig. 6a we have

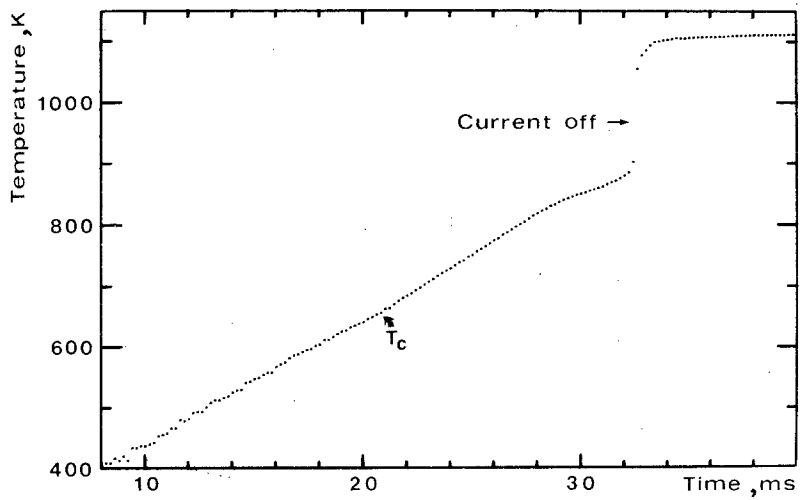

Fig. 6. Results obtained for Metglas 2605. The heating rate was 22,000 K · s^{-1}. T_c = Curie point. (a, *above*) Temperature vs time. (b, *opposite*) Electrical resistance and heat capacity vs temperature.

included the entire region of self-heating as an example. Other alloys behave similarly. In Fig. 8a the temperature decreases before crystallization. This phenomenon is probably due to specimen deformation, since all 2826 specimens proved to be U-shaped after heating.

A few specimens were examined after heating in a Rigaku/Geigerflex X-ray powder diffractometer, and for one of them (2826A, Fig. 9) literature data are available [20, 21]. On repeated isothermal annealing, two stages of crystallization can be detected, namely, MSI at 623–648 K and MSII at 663–693 K. At temperatures above 873 K the whole structure recrystallizes to a stable stage, SIII. The same transformation stages appear in DSC scans but at higher temperatures. In the MSI region part of the original glass volume crystallizes to a fcc solid solution ($Ni_{53}Fe_{47}$). In the MSII region the remaining glass forms a bct structure. The final stage at SIII consists of a fcc phase (similar to the one present in MSI), a bct phase, and an orthorhombic phase. In our X-ray diffraction recording, three peaks can be identified as fcc reflections. Three other peaks can be bct reflections, but some remaining small peaks have not been identified. Lattice parameter data are compiled in Table III. Figure 9 does not reveal the c_p and resistance change associated with the crystallization stages MSI and MSII [21], and we conclude that the major part (or all) of the crystallization takes place at temperatures above 973 K. It is reasonable to assume that we have bypassed MSI and MSII so that SIII has formed directly from the glass, and this hypothesis is confirmed, within experimental error, by the lattice parameter data.

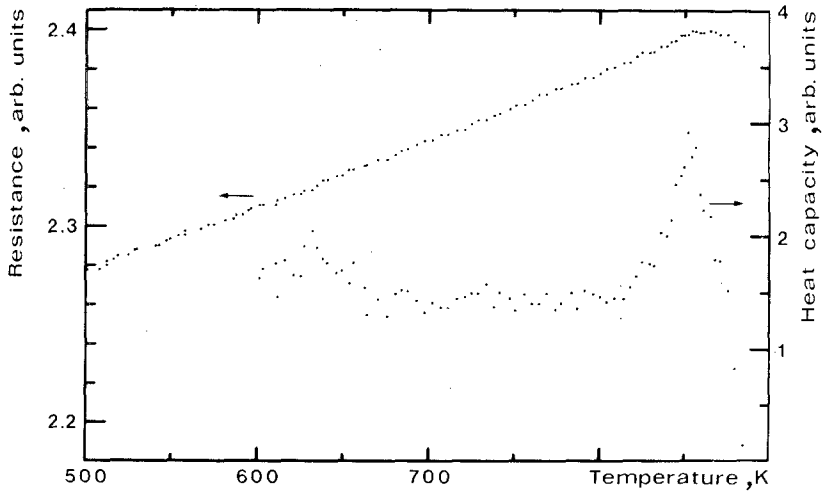

Fig. 6b.

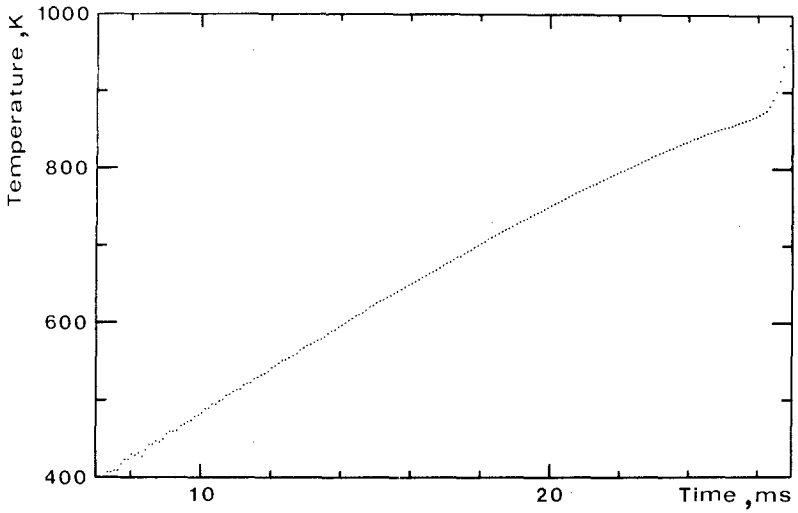

Fig. 7. Results obtained for Metglas 2605CO. The heating rate was 26,000 K · s^{-1}. (a, *above*) Temperature vs time. (b, *opposite*) Electrical resistance and heat capacity vs temperature.

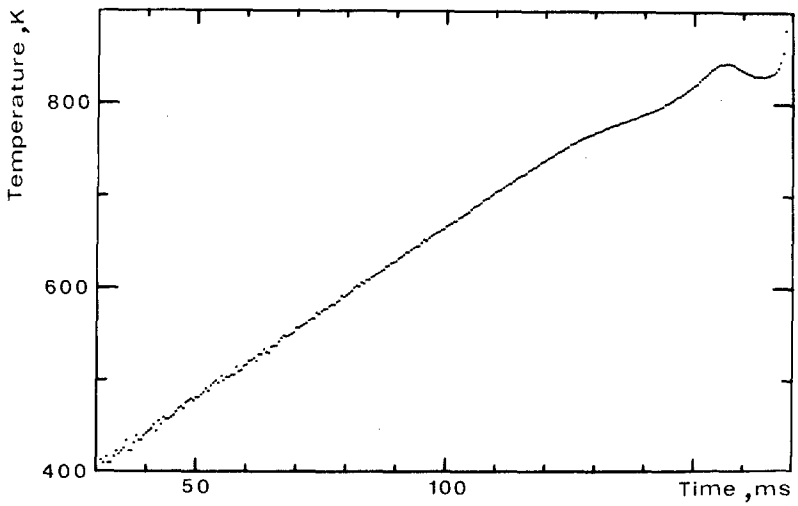

Fig. 8. Results obtained for Metglas 2826. The heating rate was 3700 K · s^{-1}. T_c = Curie point. (a, *above*) Temperature vs time. (b, *opposite*) Electrical resistance and heat capacity vs temperature.

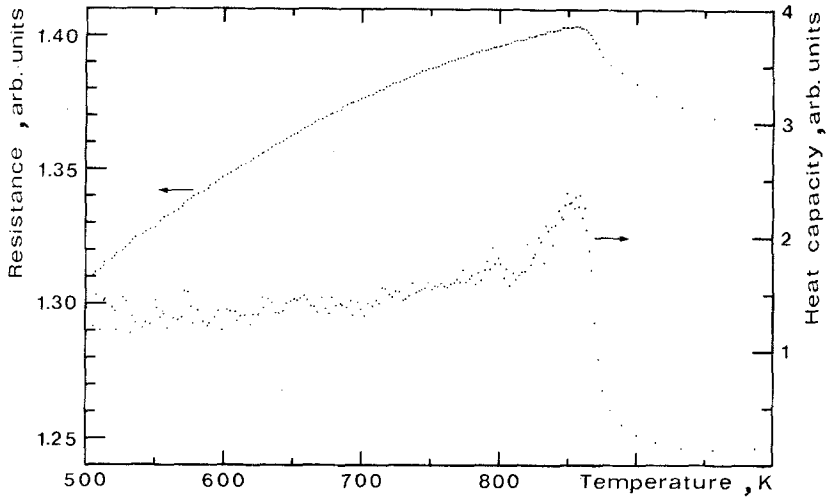
Resistance , arb. units
1.40
1.35
1.30
1.25
500
600
700
800
Temperature , K
Heat capacity , arb. units
4
3
2
1

Fig. 7b.

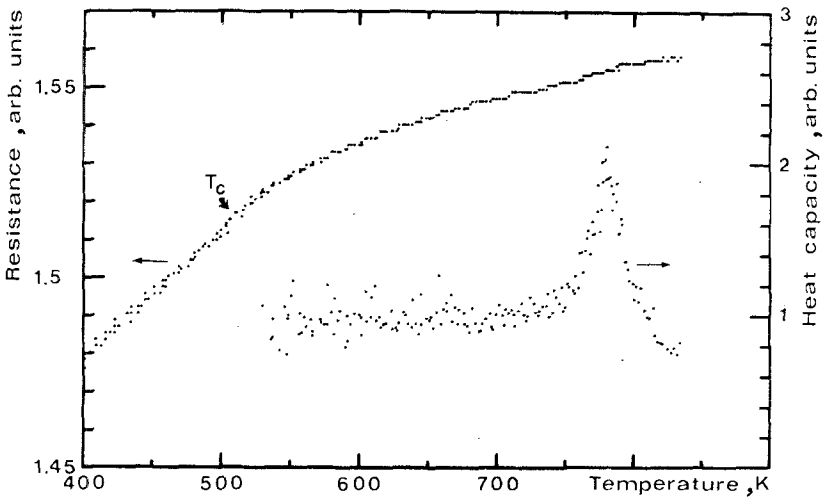
Resistance , arb. units
1.55
1.5
1.45
400
500
600
700
Temperature , K
Tc
Heat capacity , arb. units
3
2
1

Fig. 8b.

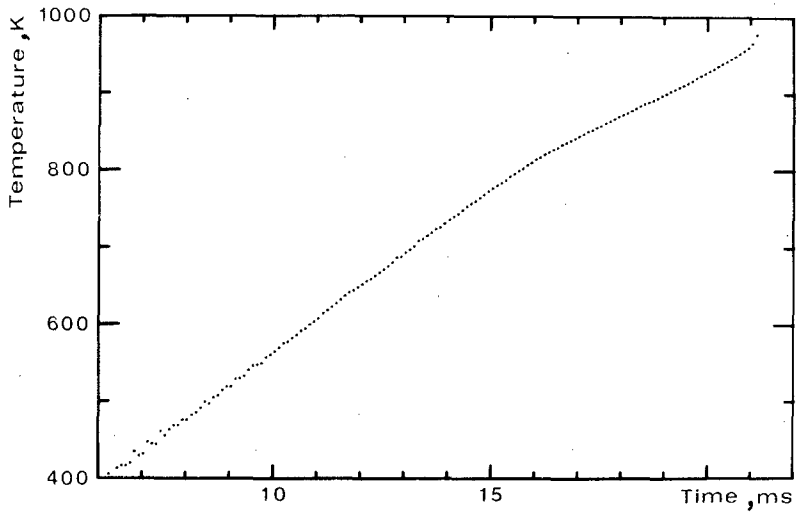

Fig. 9. Results obtained for Metglas 2826A. The heating rate was 42,000 $K \cdot s^{-1}$. (a, *above*) Temperature vs time. (b, *opposite*) Electrical resistance and heat capacity vs temperature.

Table III. Lattice Parameters (nm) of Crystalline Phases in Metglas 2826A

Stage of crystallization	Structure	von Heimendahl and Maussner [20]	Sostarich and Golenia [21]	Present work
MSI	fcc a	0.359 ± 0.002	0.3588	
MSII	fcc a	0.359 ± 0.002	0.3579	
	bct a	0.895 ± 0.003	0.8919	
	c	0.438 ± 0.003	0.4419	
SIII	fcc a	0.357	0.3579	0.3574 ± 0.0005
	bct a	0.900	0.8983	0.896 ± 0.002
	c	0.444	0.4436	0.442 ± 0.003

6. CONCLUSIONS

The temperature range covered in this work is often referred to as unaccessible to high speed thermophysical measurements. Recordings of temperature versus time, resistance versus temperature, and specific heat versus temperature have been obtained for heating rates in the range 250–42,000 $K \cdot s^{-1}$. Rough viscosity measurements have been made between glass transition and crystallization. At sufficiently high heating rates,

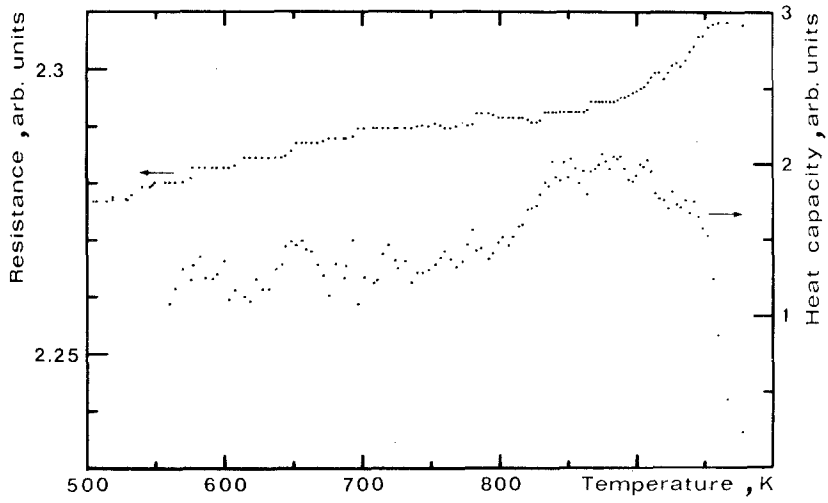

Fig. 9b.

the formation of metastable crystalline phases is bypassed, and the stable phases form directly from the amorphous state. The range of heating rates may be extended in both directions. By the use of higher current, it will probably be possible to record temperature versus time at heating rates high enough to bypass the crystallization, i.e., proceed from glass via supercooled liquid to equilibrium liquid. It would then be possible to establish temperature-time-transformation diagrams for many amorphous alloys. The present accuracy of the temperature calibration is never better than ± 15 K, but may perhaps be improved using one of the methods outlined.

ACKNOWLEDGMENTS

We wish to express our thanks to the Swedish Natural Science Research Council for financial support of the project and to Allied Chemical Corp. for test samples. Thanks are due to Miss Margit Fredriksson for performing X-ray diffraction recordings.

REFERENCES

1. H.-J. Güntherodt, in *Adv. Solid. State. Phys.*, Vol. 17 (Vieweg, Braunschweig, 1977), pp. 25–53.
2. F. E. Luborsky, ed., *Amorphous Metallic Alloys* (Butterworths, London, 1983), p. 10.
3. B. Wunderlich, D. M. Bodily, and M. H. Kaplan, *J. Appl. Phys.* **35**:95 (1964).

4. Å. Fransson and G. Bäckström, unpublished work.
5. A. Cezairliyan, *High Temp.-High Press.* **1**:517 (1969).
6. A. Cezairliyan, *High Temp.-High Press.* **11**:9 (1979).
7. U. Seydel, H. Bauhof, W. Fucke, and H. Wadle, *High Temp.-High Press.* **11**:35 (1979).
8. Ya. Dikhter and S. V. Lebedev, *High Temp.* **8**:51 (1970).
9. F. Righini, L. Coslovi, and A. Rosso, in *Proc. 8th Symp. Thermophys. Prop., Vol. II: Thermophysical Properties of Solids and of Selected Fluids for Energy Technology*, J. V. Sengers, ed. (American Society of Mechanical Engineers, New York, 1982), pp. 51–61.
10. P. M. Anderson III and A. E. Lord, Jr., *J. Non-Cryst. Solids* **37**:219 (1980).
11. H. S. Carslaw and J. C. Jaeger, *Conduction of Heat in Solids*, 2nd ed. (Oxford University Press, London, 1959), pp. 466–477.
12. A. Cezairliyan, ref. 5, p. 519.
13. B. Hopstadius, R. G. Ross, and G. Bäckström, *Phil. Mag., Part B* **47**:L89 (1983).
14. Y. S. Touloukian and D. P. DeWitt, *Thermophysical Properties of Matter, Vol. 7: Thermal Radiative Properties, Metallic Elements and Alloys* (IFI/Plenum, New York, 1970), pp. 22a–29a.
15. A. L. Greer, *Thermochim. Acta* **42**:193 (1980).
16. H. S. Chen, *J. Non-Cryst. Solids* **27**:257 (1978).
17. F. E. Luborsky, ed., ref. 2, p. 178.
18. H. S. Chen and D. Turnbull, *J. Chem. Phys.* **48**:2560 (1968).
19. T. Takamori, T. Mizosuchi, and T. R. McGuire, *Mater. Res. Bull.* **15**:81 (1980).
20. M. von Hiemendahl and G. Maussner, *J. Mater. Sci.* **14**:1238 (1979).
21. M. Sostarich and W. Golenia, *Solid State Commun.* **31**:339 (1979).